



City Research Online

City, University of London Institutional Repository

Citation: Atkin, C.J. Predicting the mission performance of a retrofit Hybrid Laminar Flow Control system. Paper presented at the Aerospace Aerodynamics Research Conference, 2002.

This is the draft version of the paper.

This version of the publication may differ from the final published version.

Permanent repository link: <https://openaccess.city.ac.uk/id/eprint/14202/>

Link to published version:

Copyright: City Research Online aims to make research outputs of City, University of London available to a wider audience. Copyright and Moral Rights remain with the author(s) and/or copyright holders. URLs from City Research Online may be freely distributed and linked to.

Reuse: Copies of full items can be used for personal research or study, educational, or not-for-profit purposes without prior permission or charge. Provided that the authors, title and full bibliographic details are credited, a hyperlink and/or URL is given for the original metadata page and the content is not changed in any way.

City Research Online:

<http://openaccess.city.ac.uk/>

publications@city.ac.uk

Predicting the cruise performance of a retrofit Hybrid Laminar Flow Control system

C J Atkin, Aerodynamics Department, QinetiQ Ltd, Farnborough

W J A Courtenay, Department of Engineering, Cambridge University

Abstract

A technique is presented for assessing the cruise performance of an aircraft employing a hybrid laminar flow control (HLFC) system. Two-dimensional HLFC designs based on N-factor control of chamber pressures are extrapolated to a complete aircraft, leading to a full analysis of the potential drag reduction as well as the system power and weight penalties. These can remove over 30% of the aerodynamic drag benefit delivered by laminar flow. Simple trapezium-shaped suction distributions reduce the benefit still further, but the use of non-local stability methods would suggest a reduction of nearly 25% in suction requirements, increasing the net drag benefit by 10%. Modifications to the wing geometry indicate that changes favourable to laminar flow nevertheless introduce unacceptably large wave drag penalties. The most promising direction for future research appears to be extending the extent of the suction control system. Extrapolating the predicted HLFC system performance to the entire wing upper surface, horizontal tail plane and fin would suggest a potential 6½ - 7% reduction of total aircraft drag for the A310 at maximum L/D .

Notation

c_p	Specific heat capacity at constant pressure	$\eta_{a/c}$	Overall aircraft efficiency
$C_{L,a/c}$	Aircraft lift coefficient	η_{isen}	Isentropic efficiency of pumping process
$C_{L,sec}$	Sectional lift coefficient	η_{mech}	Mechanical efficiency of pump
$C_{L,wf}$	Lift coefficient of wing-fuselage combination	η_{motor}	Efficiency of pump motor
u	velocity	η_{off}	Efficiency of engine power offtake process
h	enthalpy	η_{pump}	Overall efficiency of pump = $\eta_{mech} \times \eta_{isen}$
\dot{m}	suction mass flow rate		
M	Mach number		Subscripts:
T	temperature	w	at the wing surface
p	pressure	i	at the pump inlet
Pr	Prandtl number	x	at the pump exhaust
γ	Ratio of specific heats	0	stagnation conditions
		∞	in the free stream

1. Viscous drag reduction for an HLFC retrofit aircraft

The previously-reported work [2] focussed on the application of robust and automated stability analysis tools to the design of discrete suction chamber layouts for a Hybrid Laminar Flow Control wing *section* based on the concept of N-factor control targets. The objective of the present study was to extend the analysis to a three-dimensional wing and to assess the potential drag reduction for the complete aircraft.

1.1 Outline of the approach

Since the methods used for HLFC design are still very much restricted to quasi-two-dimensional flows (infinite-yawed or swept-tapered wings) the coupling of these methods with a fully three-dimensional CFD method was not considered. Instead, use was made of an existing 2D-to-3D method [4] developed at QinetiQ to construct a three-dimensional wing model from a database of quasi-two-dimensional results. As with previous work [2] it is assumed that the behaviour of the outer part of the wing can be modelled using a single representative wing section, Figure 1.

Unlike the previous studies, the effect of the loading, $C_{L,sec}$, and Reynolds number variation along the span must now be taken into account. In principle (for the fully-turbulent case) Reynolds number dependence can be treated using simple power laws to scale the friction, form and wave drag. In this way the variation of the flowfield along the wing span can

be obtained from a single lift-drag polar for the reference wing section. When there is a significant region of laminar flow the drag varies with Reynolds number in a non-trivial way. However the same 2D strip approach can be followed by calculating a series of polars for HLFC sections at different Reynolds numbers — Reynolds number sensitivity is then obtained from a database of results rather than from simple power laws.

Variation in overall aircraft lift coefficient, $C_{L,a/c}$, can also be accommodated in this way without any further calculations, but variations in cruise Mach number would clearly require the calculation of additional polars. Additionally, because of the presence of the suction system, the influence of altitude is more complex than a simple Reynolds number effect, so the 2D-to-3D analysis would have to be repeated for different cruise altitudes.

1.2 Transformation to 3D

The first step of the transformation process is to analyse the baseline (turbulent) configuration at a given cruise altitude and Mach number. The representative wing section must be transformed into an 'equivalent' two-dimensional aerofoil prior to calculating a 2D lift-drag polar. (The 2D viscous full potential code "BVGK" was used in the present work: BVGK not only calculates the 2D flowfield but also determines the lift, pitching moment and drag coefficients, the latter decomposed into friction, form and wave drag components.) At this stage, transition is set at 1% chord representing a standard 'turbulent wing' design and the 2D Reynolds number is set to a typical mid-span value.

The 2D-to-3D transformation code uses a simple outline of the wing and fuselage planform geometry to define the spanwise distribution of section lift coefficient $C_{L,sec}$ and Reynolds number for each of a series of wing-fuselage lift coefficients $C_{L,w/f}$. At each spanwise station the 2D lift-drag polar is used to determine the local pitching moment and drag coefficients corresponding to the local $C_{L,sec}$, with transformations to and from the equivalent two-dimensional flow being invoked as required. The turbulent drag coefficients are scaled using simple power laws to match the local section Reynolds number.

The sectional pitching moment and drag distributions are then integrated over the span to give values for the wing-fuselage combination. These are then corrected empirically for additional factors, such as wing-off and interference drag, tail area and tail arm, to give overall coefficients for the trimmed aircraft. Repeated analyses at different values of $C_{L,w/f}$ yield a final lift-drag polar for the complete aircraft, $C_{D,a/c}$ versus $C_{L,a/c}$. Clearly there is a degree of empiricism built in to this approach, but the important point is that, by following the same procedure for the HLFC case, a sensible *comparison* can be made between the turbulent and HLFC aircraft.

The 2D-to-3D transformation procedure is modified for HLFC cases as follows: at each spanwise station, the code determines whether the section is inside or outside the HLFC spanwise range defined by the user. If outside this range, the code uses the fully-turbulent 2D polar as before to calculate the correct pitching moment drag and coefficients for the local section. If inside the HLFC range, the code makes use of a database of additional 2D HLFC polars, supplied by the user, to obtain coefficients appropriate to the local sectional Reynolds number. The HLFC polars are calculated in the same way as the turbulent polars with transition set further aft: the precise transition position is obtained for each 2D case from the HLFC chamber design tool [2]. The application of the chamber design procedure to all these cases is the expensive part of the analysis. Since each combination of chamber layout, $C_{L,sec}$, Reynolds number, Mach number and cruise altitude requires a separate sectional HLFC analysis, a certain amount of scoping must be done to establish the minimum number of combinations required for acceptable accuracy. This is discussed further below.

1.3 HLFC analysis

Purely from the point of view of efficiency, some limits have to be applied to the size of the database of 2D flows used in the analysis of each configuration. The following constraints were applied in the present work, and seemed to limit the effort involved in the analysis without compromising either the accuracy nor the significance of the results. First, a fixed chamber layout (i.e. chamber positions scaling with local chord) was imposed for a given configuration. Second, following a thorough investigation, it became clear that the minimum number of $C_{L,sec}$ values required to resolve adequately the 2D lift-drag behaviour was as small as four (including a zero-lift case which could be common to both turbulent and HLFC polars). Third, spanwise variations in Reynolds number were treated by calculating polars at only two spanwise sections, the inboard and outboard extremes of the HLFC region, and using simple interpolation to obtain results for intermediate values. Fourth, the cruise Mach number was fixed at the design value for the A310 aircraft, namely 0.8. Fifth, as with local Reynolds number variation, altitude effects were handled by analysing each configuration at two extremes of altitude, typically 10,000 ft apart. This gave a total of twelve quasi-two-dimensional HLFC cases, or four polars (two per cruise altitude), for each configuration.

The chamber design tool [2] was used to determine chamber pressures, mass flow rates and an upper surface transition position for each of these twelve cases. The required surface pressure distributions were obtained from the initial, fully-

turbulent polars. As an experiment, some of the surface pressures obtained from the HLFC polars (i.e. after delayed transition positions had been determined) were re-submitted to the chamber design tool: the effect on the suction rates and transition positions was small (less than 1%), so it was not felt necessary to standardize on this procedure.

1.4 Results at maximum lift-drag ratio

The following paragraphs present the results for the aerodynamic analysis of the A310 aircraft with a part-span HLFC retrofit (between 50% and 90% semi-span) on the wing *upper surface* only. First of all Figure 2 illustrates the variation of $C_{L,sec}$ along the span of the wing at an aircraft $C_{L,a/c}$ close to maximum L/D . Note that $C_{L,sec}$ is here based on *local* wing chord — a distribution based on *mean* chord would be more obviously recognizable as a nearly elliptic distribution. Here the loading was determined from both elliptic loading and wing-root bending moment requirements. The purpose of the figure is to highlight the mean value of $C_{L,sec}$ in the 50%-90% semi-span range of about 0.58. This value was chosen for the sectional lift-drag polars, along with 0.46 and 0.70, some 20% above and below this mean value. Pressure distributions for these three conditions are illustrated in Figure 3.

The spanwise distribution of drag reduction is shown in Figure 4, this time non-dimensionalized with mean chord rather than local chord. The observed reduction in viscous drag over the HLFC span (about 20%) is consistent with a rough estimate of 0.3 (delay in transition of 30% chord) \times 0.67 (the proportion of viscous drag associated with the upper surface) \approx 0.2.

Finally, the overall effect is summarised in Figure 5 which focusses on the area around maximum L/D . The actual values of L/D cannot be published, but the difference represents an improvement in maximum L/D of 1.58% — this from laminarization of about 8½% of the wing upper surface. The results below were obtained at 29,000 ft: the drag reduction at 39,000 ft is similar, but the overall aircraft drag coefficient is slightly greater, and the net benefit is 1.46%.

2. Pump drag analysis

The next task is to estimate the suction system power requirement and the effect on the overall aircraft performance, preferably in terms of an effective 'pump drag'. The analysis focusses on a control volume which encloses the pumped air from its initial state, in some notional streamtube ahead of the wing, to its final state as an exhaust jet, Figure 6.

2.1 Pump power consumption and exhaust thrust

If the pumping process is adiabatic, the steady flow energy equation yields the following expression connecting the enthalpy rise with the pump shaft power, mechanical efficiency and suction mass flow rate:

$$h_{0x} - h_{0i} = c_p (T_{0x} - T_{0i}) = \frac{\eta_{mech}}{\dot{m}} P_{shaft} \quad 2-1$$

T'_{0x} , the **isentropic** total temperature at exhaust, is defined by the relation

$$\eta_{isen} = \frac{T'_{0x} - T_{0i}}{T_{0x} - T_{0i}} \quad 2-2$$

and yields an expression for the change in total pressure:

$$\frac{p_{0x}}{p_{0i}} = \left(\frac{T'_{0x}}{T_{0i}} \right)^{\frac{\gamma}{\gamma-1}} = \left[1 + \eta_{isen} \left(\frac{T_{0x}}{T_{0i}} - 1 \right) \right]^{\frac{\gamma}{\gamma-1}} \quad 2-3$$

so that, substituting into equation 2-1 and expanding the total pressure at exhaust, we obtain

$$P_{shaft} = \frac{\dot{m} c_p T_{0i}}{\eta_{pump}} \left[\left(\frac{p_x}{p_{0i}} \right)^{\frac{\gamma-1}{\gamma}} \left(1 + \frac{\gamma-1}{2} M_x^2 \right) - 1 \right] \quad 2-4$$

where the isentropic and mechanical efficiencies are combined into a single value for the pump. Now the exhaust stream is considered some distance downstream of the system such that $p_x = p_\infty$, so that the resultant thrust force is then equal to the rate of change of momentum of the air

$$F_{pump} = \dot{m}(u_x - u_\infty) \quad 2-5$$

2.2 Net pump drag

For a standard aircraft the power consumption in cruise is related to drag as follows:

$$P_{a/c} = \frac{u_\infty D_{aero}}{\eta_{a/c}} \quad 2-6$$

Including the power requirement and thrust effect of the HLFC suction, the modified power consumption becomes

$$P'_{a/c} = \frac{u_\infty (D_{aero} - F_{pump})}{\eta_{a/c}} + \frac{P_{shaft}}{\eta_{off} \eta_{motor}} = \frac{u_\infty (D_{aero} + D_{pump})}{\eta_{a/c}} \quad 2-7$$

where η_{off} and η_{motor} cover losses in the power offtake and pump drive. Rearranging for D_{pump} , the 'pump drag',

$$D_{pump} = \frac{\eta_{a/c}}{\eta_{off} \eta_{motor}} \frac{P_{shaft}}{u_\infty} - F_{pump} \quad 2-8$$

Substituting equations 2-4 and 2-5 into the above expression and putting $p_x = p_\infty$, gives:

$$D_{pump} = \left[\frac{\eta_{a/c} / \eta_{off}}{\eta_{motor} \eta_{pump}} \right] \frac{\dot{m}_c p_{T0i}}{u_\infty} \left[\left(\frac{p_\infty}{p_{0i}} \right)^{\frac{\gamma-1}{\gamma}} \left(1 + \frac{\gamma-1}{2} M_x^2 \right) - 1 \right] - \dot{m} (u_x - u_\infty) \quad 2-9$$

The most obscure quantity in equation 2-9 is the power offtake ratio $[\eta_{a/c}/\eta_{off}]$. The aircraft efficiency is defined as

$$\eta_{a/c} = \frac{u_\infty Thrust}{\dot{m}_{fuel} Q} \quad 2-10$$

where Q represents the calorific value of the fuel, while the offtake efficiency is defined as

$$\eta_{off} = \frac{P_{off}}{\Delta \dot{m}_{fuel} Q} \quad 2-11$$

so that

$$\frac{\eta_{a/c}}{\eta_{off}} = \frac{u_\infty Thrust}{P_{off}} \frac{\Delta \dot{m}_{fuel}}{\dot{m}_{fuel}} = u_\infty Thrust \left[\frac{\Delta sfc}{sfc P_{off}} \right] \quad 2-12$$

where the factor in square brackets, the change in specific fuel consumption (*sfc*) for a particular level of power offtake, seems to be the industry-standard method of defining offtake performance.

2.3 Results at maximum lift-drag ratio

The key parameters in determining the pump drag penalty are the total mass flow rate and the increase in total pressure required from pump inlet to pump exhaust. These quantities need to be determined from the series of 2D HLFC section designs used in the prediction of aerodynamic performance above. Although the resulting suction chamber plenum pressures were by no means uniform, the present analysis was simplified by assuming that the streams from all chambers would be throttled down to the lowest common pressure. The problem of $C_{L,sec}$ variation across the span was mitigated by the fact that, at the lower value of lift coefficient, both chamber pressures *and* mass flow rates were lower — the converse being true at the higher value of $C_{L,sec}$. The resulting variation in pump drag was less than 4%, so that the mass flow and chamber pressure figures for $C_{L,sec} = 0.58$ were taken as representative of the whole wing. Finally, Reynolds number variation across the span was treated by *averaging* the local values of mass flow rate at mid-span and tip, while taking the *minimum* of the chamber plenum pressures.

Pump and motor efficiencies were obtained by comparing shaft power and negative thrust figures (equations 2-4 and 2-5) with data generated for the HYLTEC project by AoA Gauting ([3], [5]) — this also provided an opportunity to validate the trends given by these relations, which matched the performance of the real components very closely. More difficulty was encountered in finding figures for the relative power offtake efficiency, but the value $[\eta_{a/c}/\eta_{off}] = 0.8$ was used in the present study (i.e. power offtake was assumed to be more efficient than the propulsive process).

Using equation 2-9 above with an exhaust Mach number of 0.2 (recommended during the HYLTEC project as providing a good balance between pump drag penalty and additional size and weight, [5]), then the pump drag penalty for a six-chamber layout designed using the approach described in [2] is 0.24% of total drag at maximum L/D , Mach 0.8, 29,000 ft. This compares with the aerodynamic drag reduction of 1.58% — so that the pump drag penalty reduces the HLFC benefit by about one sixth.

The pump drag analysis provides a useful quantitative comparison between the chamber-based suction system design proposed by the author, Figure 7, and a chamber layout which aims to reproduce a simple trapezium-shaped distribution of suction, Figure 8. Although the corresponding N-factor distributions, Figure 9 and Figure 10, both satisfy the same N-factor control requirement, the latter approach requires nearly 50% more mass flow (which does not improve the transition position), and the positioning of a chamber under the upper surface suction peak means that the required pump pressure rise is also greater. The calculated pump drag for the trapezium-suction distribution here amounts to 0.40% of total aircraft drag at maximum L/D , over one quarter of the HLFC benefit.

A popular issue among the HLFC research community is the optimization of exhaust Mach number to reduce the overall pump drag. In the case of unit efficiencies, the classical optimum condition in which the exhaust velocity is equal to the free stream velocity can be derived easily from equation 2-9. However the effect of losses in the system is to flatten considerably the minimum in the pump-drag-versus-exhaust-Mach-number relation. Thus, for example, the pump drag penalty for the A310 case discussed above is 0.24% at an exhaust Mach number of 0.2, but this only drops to a minimum of 0.22% when the exhaust Mach number is increased to 0.63 — this is assuming the pump efficiency to be independent of exhaust Mach number, which may not be the case [5]. Since the overall impact of pump drag is rather small — *for a well-designed system* — optimising exhaust velocity from a perspective of *drag* alone may be misleading since the exhaust velocity requirement also determines the size and *weight* of the required pump. These factors would impact significantly upon the ease of installation as well as the overall aircraft aerodynamics.

3. System weight considerations

One remaining factor to be considered is the weight penalty associated with the ducting, pump and control equipment required for the suction system. Since the present work is concerned with changes in drag, it was thought useful to express the suction system weight estimates obtained during the HYLTEC project [3] as additional drag penalties. This was done by considering the lift-drag trade-off at maximum L/D :

$$\Delta C_{D,cruise} \approx \frac{\Delta m}{m_{cruise}} \frac{C_{L,cruise}}{[L/D]_{cruise}} \tag{3-1}$$

Applying this relationship to the weight figures quoted in [3] suggests that an additional penalty of 0.20% total aircraft drag should be taken into account when assessing the overall impact of the HLFC system. For the baseline A310, the aerodynamic drag reduction of 1.58% then becomes a net drag benefit of 1.14%. For the case of the trapezium suction distribution, assuming that the system weight scales with the suction mass flow rate, the net benefit is only 0.89%.

4. Effect of constrained design modifications on HLFC performance.

In addition to the analysis of an HLFC retrofit to the baseline A310 wing, an investigation was conducted into a number of modifications to the wing section and their effect on the performance of both the turbulent and HLFC aircraft.

4.1 Wing geometry modifications.

The following geometry modifications were tested:

- a. a reduction of 2° in leading edge sweep;
- b. a reduction in nose thickness given by equation 4-1; and
- c. a positive 'flap' deflection given by equation 4-2.

The following transformations were used:

$$\left. \begin{aligned} \text{(b)} \quad \frac{z'}{c} &= \frac{z}{c} \left[1 - \varepsilon \left(\frac{x}{x_0} - 1 \right)^3 \right] \quad \text{for } \frac{x}{c} \leq 0.2 \\ &\quad \varepsilon = 0.1 \end{aligned} \right\} \tag{4-1} \quad \left. \begin{aligned} \text{(c)} \quad \frac{x'}{c} &= 0.8 + \left(\frac{x}{c} - 0.8 \right) * \cos \delta \\ \frac{z'}{c} &= \frac{z}{c} - \left(\frac{x}{c} - 0.8 \right) * \sin \delta \end{aligned} \right\} \text{for } \frac{x}{c} \geq 0.8 \quad \delta = 2^\circ \tag{4-2}$$

The sweep reduction was expected to reduce the control requirements for crossflow instability. Both the section modifications resulted in moving the loading further aft, reducing the amplification of Tollmien-Schlichting waves downstream of the suction control region. In all cases the shock was slightly strengthened, as expected.

The results of these changes are summarised in Table 1 below. All the geometry modifications result in wave drag increases which are not negligible compared to the HLFC benefit. The other effect of the sweep reduction is indeed to reduce the amount of suction power (and therefore pump drag) required by about 9%, without much impact on the amount of laminar flow. Since the pump drag penalty amounts to only 16% of the overall HLFC benefit, this further improvement is perhaps insufficient to justify the effort of changing the wing geometry. The nose geometry modification has a significant impact upon viscous drag saving since transition can be delayed much further, to 38% chord or beyond. This is due to the more favourable pressure distribution which, unfortunately, is also the origin of the wave drag increase. The trailing edge deflection yields very little benefit, except to allow transition to be pushed further aft if additional suction is applied.

In general, although there is some increase in laminar area, most of these modifications result in significant wave drag penalties while making little impact upon the overall drag balance — certainly not enough to consider the cost of implementing such a geometry modification. This is interesting, and may prove to be a general rule with today's advanced wing section designs which are highly-optimised from the point of view of wave drag. Admittedly, the balance might change if a greater span of the wing were laminarized, but it appears from these studies that far more benefit is likely to come from extending the suction control region further downstream than by trying to pursue a 'laminar flow section' design philosophy for future HLFC applications.

Summary of A310 HLFC wing retrofit results						
Case no.	Details of any geometry modification	HLF analysis details	Δ CD (Aero) %total	Δ CD (Pump) %total	Δ CD (Weight) %total	Δ CD (net) %total
1T	Baseline	Turbulent baseline investigated at 29,000 ft, Mach 0.8, using a 2D->3D analysis at maximum L/D.	0.00%			
1L	Baseline	HLFC on upper surface between 50% and 90% semi-span. Transition between 29% - 34% chord.	1.58%	0.24%	0.20%	1.14%
2T	Reduced sweep	As for case 1T.	-0.68%			
2L	Reduced sweep	As for case 1L. Transition between 31% - 42% chord.	1.12%	0.21%	0.20%	0.71%
3T	Reduced nose thickness	As for case 1T.	-0.42%			
3L	Reduced nose thickness	As for case 1L. Transition between 29% - 46% chord.	1.67%	0.17%	0.20%	1.30%
4T	Negative flap	As for case 1T.	-0.59%			
4L	Negative flap	As for case 1L. Transition between 22% - 32% chord.	1.09%	0.24%	0.20%	0.65%
4Lx	Negative flap	As for case 4L. Transition pushed 4-5% aft at higher CLs.	1.28%	0.25%	0.20%	0.83%

Table 1: summary of HLFC benefit, pump drag penalty and net benefit for baseline A310 and various modifications.

5. Impact on predicted HLFC performance of aerodynamic assumptions and tools

Finally, having seen that the suction system specification can almost halve the aerodynamic benefit, it is interesting to see how the use of more advanced, though relatively untried methods would impact upon the design process. The

chamber design tool [2] was modified to use the Imperial College PSE method [6] rather than the classical e^N method in use at QinetiQ. The PSE method was used as a linear stability tool, producing non-local N-factors, which were controlled in the same way as previously. Clearly, one of the major issues with linear PSE methods is that the N-factors have not yet been successfully calibrated against experimental data. Non-local N-factors are known to be marginally higher than classical N-factors for most modes of instability, but for crossflow modes in the region of the wing leading edge they predict significantly lower amplification rates. This is demonstrated by the application of the modified chamber design method to one of the HLFC section cases ($C_{L,sec}$ of 0.58 at the mid-span position, Mach 0.8, 29,000 ft). Non-local N-factors are plotted in Figure 11: these can be compared with the classical N-factors in Figure 9, and it can be seen that the N-factor control is broadly similar. The chamber pressures in Figure 12 however, are decidedly different from those shown in Figure 7. The control requirement in the leading edge region has been significantly reduced, even necessitating a reduction in chamber sizes to allow the reduced mass flow rates to be achieved. The net effect is a 24% reduction in mass flow rate and therefore pump drag and weight penalties of only 0.18% and 0.15% of total aircraft drag at maximum L/D . The net HLFC benefit increases from 1.13% to 1.25%. Perhaps a more significant advantage is that the suction rates near the leading edge are much further from the over-suction limits discussed in [2]: this would mean that the suction system design would involve far less risk of failure by over-suction.

6. Conclusions

The HLFC wing section designs of previous studies have been successfully combined, using a 2D-to-3D transformation tool, to allow the performance of a complete wing with part-span HLFC retrofit to be assessed.

For a laminarized area equal to 8½% of the wing upper surface, an aerodynamic drag benefit of 1.6% total aircraft drag is predicted at maximum L/D . System weight and power requirements suggest that the net benefit would be reduced to 1.1% total aircraft drag.

Trapezium-based suction distributions would see this benefit reduced still further to 0.9%, while the use of non-local stability methods (such as linear PSE) would suggest a reduction in suction requirements, increasing the net benefit to 1.3% of total aircraft drag.

Modifications to the wing geometry indicate that changes favourable to laminar flow nevertheless introduce unacceptably large wave drag penalties.

The most promising direction for future design research appears to be extending the extent of the suction control system in both spanwise and chordwise directions, and to other parts of the airframe: the surface area subjected to HLFC retrofit in the present study amounts to only 18% of the combined area of wing upper surface, horizontal tailplane and fin on the A310 aircraft. A similar HLFC performance in all these areas would suggest a potential 6½ - 7% reduction of total aircraft drag for the A310 at maximum L/D .

7. References

- 1 Bieler H. *HYLTEC Hybrid Laminar Flow Technology. Annex 1: Project Programme*, EU contract no. BRPR-CT97-0606, November 1997.
- 2 Atkin C J. *New Aerodynamic Approach to Suction System Design*, DragNet European Drag Reduction Conference, Potsdam, June 2000.
- 3 Möller W, Sturm H, Pfennig J. *HYLTEC Task 2.2.3: Development of system parameters: system layout*. HYLTEC Technical Report no. 21, parts A & B, June 2000 & March 2001.
- 4 Hackett K C. *Private communication*. August 2001.
- 5 Sturm H. *Private communication*. September 2001.
- 6 Mughal M S, Hall P. *Parabolized stability equations and transition prediction for compressible swept-wing flows*. Imperial College Report, November 1996.

8. Figures

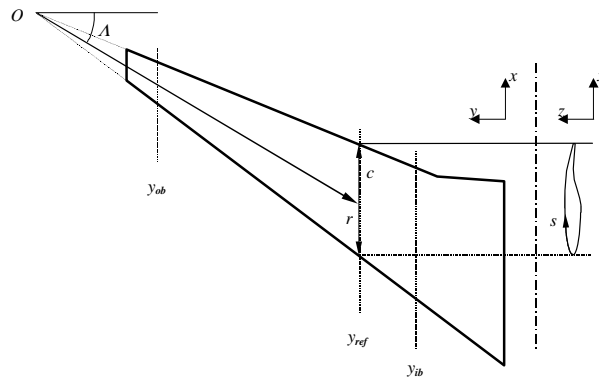


Figure 1: Wing planform and section illustrating limits of outer wing suction control.

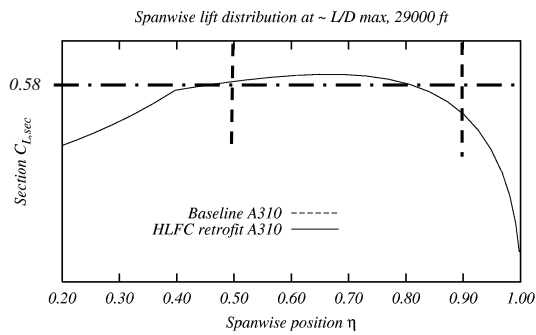


Figure 2: spanwise variation of section C_L .

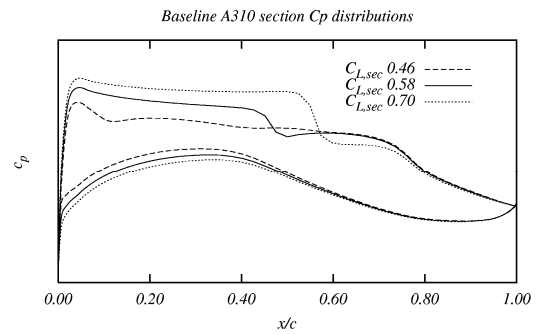


Figure 3: c_p distributions at different section C_L s.

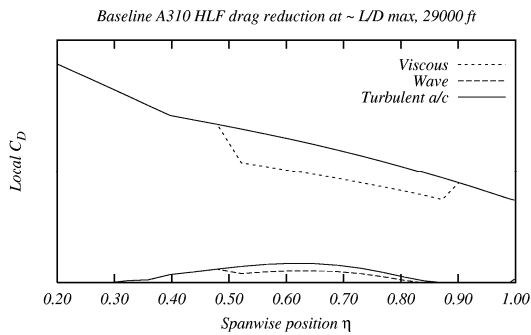


Figure 4: spanwise distribution of drag reduction.

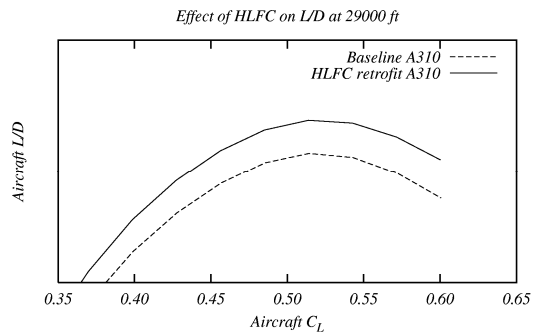


Figure 5: effect of HLFC retrofit on overall L/D.

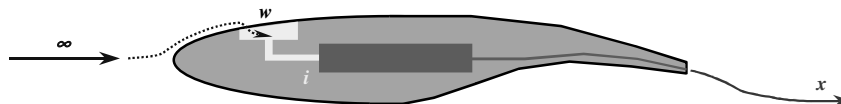


Figure 6: schematic of pumped air flow process.

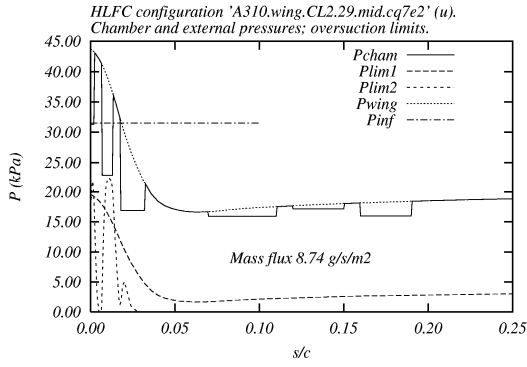


Figure 7: suction system obtained using the chamber design tool [2].

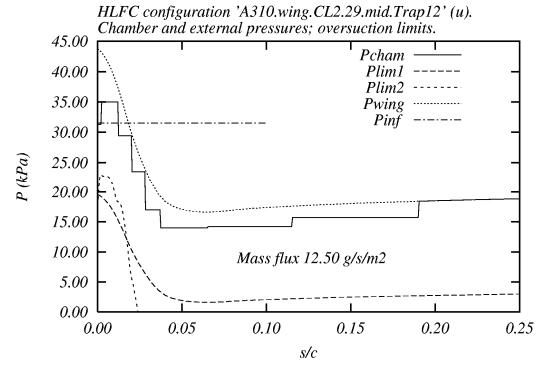


Figure 8: suction chamber pressures selected to mimic a trapezium velocity distribution.

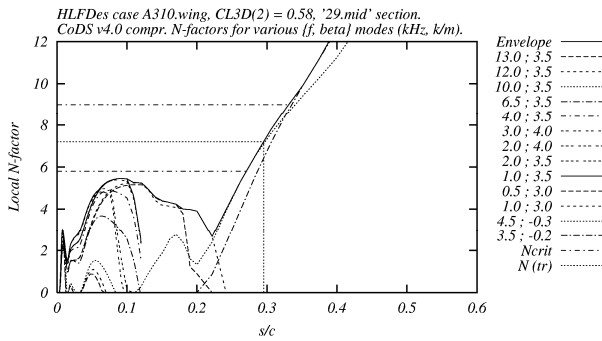


Figure 9: N-factors for A310 HLFC retrofit system designed using the chamber design tool.

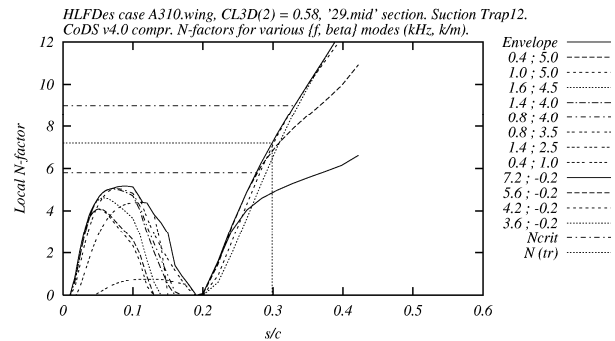


Figure 10: N-factors for A310 HLFC retrofit system using the trapezium distribution in Figure 8.

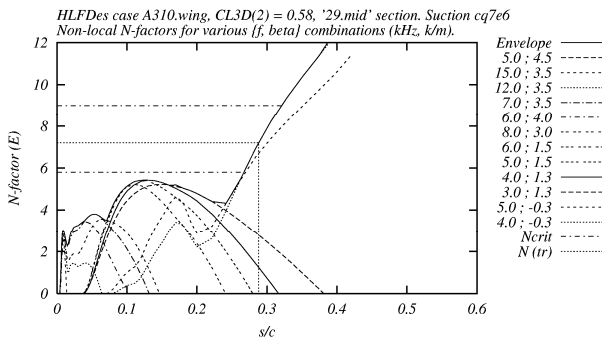


Figure 11: N-factors for A310 HLFC retrofit system designed using non-local N-factors.

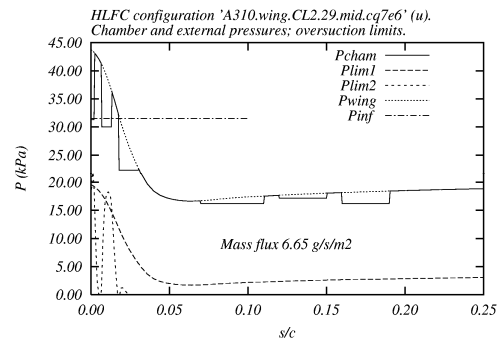


Figure 12: chamber pressures for A310 HLFC retrofit system designed using non-local N-factors.